Energy 223 (2021) 120097

Contents lists available at ScienceDirect

Energy

journal homepage: www.elsevier.com/locate/energy

Performance analysis and multi-objective optimization of the high-temperature cascade heat pump system

Zhangxiang Wu [a], Xiaoyan Wang [a], Li Sha [a], Xiaoqiong Li [a, b, *], Xiaochen Yang [a], Xuelian Ma [a], Yufeng Zhang [a]

[a] School of Environmental Science and Engineering, Tianjin University, Tianjin, 300350, PR China
[b] Technical Institute of Physics and Chemistry CAS, Key Laboratory of Equipment and Energy-saving Technology on Food & Pharmaceutical Quality Processing, Storage and Transportation, China National Light Industry, Beijing, 100190, China

ARTICLE INFO

Article history:
Received 2 September 2020
Received in revised form
6 January 2021
Accepted 9 February 2021
Available online 11 February 2021

Keywords:
High-temperature cascade heat pump system
Thermodynamic analysis
Economic analysis
Multi-objective optimization

ABSTRACT

This paper presents a high-temperature cascade heat pump system with a high compression ratio for recovering the waste heat of the chemical plant and replacing the steam. To analyze the economic and the thermodynamic performance of the high-temperature cascade heat pump, a mathematical model, considering energy, exergy, economy and environment, has been developed under different heat source inlet temperature. The proposed system here indicated good stability and feasibility under various operating conditions according to the simulation results. However, as the heating capacity and the annual net profit were found to be conflicting with each other, a multi-objective optimization method was developed to solve this problem. In addition, the technique for Order of Preference by Similarity to Ideal Solution method was selected as the decision-making method to search for the final optimal result of the system. The optimization results showed that if the optimized heating capacity project was selected, the average heating capacity and the average annual net profit were 2.8% and 6.7% lower than their maximum possible values. At the optimal heat source inlet temperature of 71 °C and condensing temperature of 145 °C, the heating capacity of the system was 498.9 kW and the payback period was 3.9 year.

1. Introduction

With economic development and population increases, energy consumption has risen rapidly in recent years [1]. The massive application of fossil fuels, including natural gas, petroleum and coal, however, has caused serious pollution and haze problems. To surmount these problems, supplying energy through renewable energy sources such as waste heat energy is one of the most effective ways of saving energy and protecting the environment. The recovery of industrial waste heat could increase the energy efficiency by 10–50% [2].

Vapor-compression high-temperature heat pump (HTHP) is a key technology of low-temperature heat recovery, which is widely applied in industrial fields, such as chemical plants, milk factories and paper mills [3,4]. It can improve low quality heat energy to high quality by consuming a small amount of electric energy or heat. At present, the single-stage heat pump system using water as refrigerant could provide the condensing heat of 150 °C [5]. However, high compression ratio will bring some negative effects (a high discharge pressure, high oil temperature, low volumetric efficiency and low coefficient of performance (COP)), resulting in the single-stage heat pump can only be used at low temperature lift (the temperature difference between the heat source and cold source) [6,7]. The proposal of high-temperature cascade heat pump (HTCHP) effectively solves these problems, expanding the application field and scope.

The HTCHP system has been widely researched in relation to its superior performance. Song et al. [8,9] analyzed the performance of CO_2/R134a cascade heat pump system for district heating from theoretical and experimental perspectives. The system could provide hot water of 50–75 °C. The theoretical results indicated that the R134a cycle played a major role in the cascade system, and the COP was improved under relatively low ambient and hot water supply temperatures [8]. The experimental results verified the

* Corresponding author. School of Environmental Science and Engineering, Tianjin University, Tianjin, 300350, PR China.
E-mail address: xiaoqiong_li@tju.edu.cn (X. Li).

https://doi.org/10.1016/j.energy.2021.120097
0360-5442/

Nomenclature

A	The area of heat exchanger (m^2)
ANP	Annual net profit ($/year)
COP	Coefficient of performance
Cl_i	proximity index
CRF	Capital recovery factor
EC	annual electrical energy consumption ($/year)
EEV	Electronic expansion valve
Ex	exergy rate (kW)
F	correction factor of the logarithmic mean temperature difference
H, h	enthalpy (kJ/kg)
HTCHP	high-temperature cascade heat pump
HTHP	high-temperature heat pump
HTS	high temperature stage
i	annual interest rate
K	Total heat transfer coefficient of heat exchanger (W/(㎡·K))
L	Exergy destruction (kW)
LTS	low temperature stage
M	Mass flow rate (kg/s)
N	annul operating hour (h)
n	life time (year)
P	Pressure (MPa)
PP	payback period (year)
Q	Heating (kW)
S	Entropy (kJ/(kg·K))
t,T	Temperature (°C)
TOPSIS	technique for order preference by similarity to an ideal solution
W	Power consumption (kW)
Z	Cost ($)
ΔT_{LMD}	logarithmic mean temperature difference (°C)

Greek symbols

φ	operation and maintenance factor
Ψ_k	exergy efficiency
η_s	efficiency of the compressor
η_{cas}	the efficiency of the cascade heat exchanger
μ_{co2}	emission factor

Subscripts

1,1′,2,2′,3,3,4,5,5′,6′,6,7,8,9,10	state point
cas	cascade heat exchanger
CI	capital investment
comp	compressor
cond, re	condenser
evap	evaporator
f	refrigerant
H	high temperature stage
L	low temperature stage
OM	operation and maintenance cost
R	Reference value

existence of the optimal discharge pressure in the subcooler-based cascade heat pump (CHP) system [9]. Bamigbetan et al. [10] experimentally investigated a prototype compressor of the high temperature stage (HTS) in the CHP system with propane in the low temperature stage (LTS) and butane in the HTS. They found that the total compressor efficiency was 74% and the volumetric efficiency was 83% [10]. The performance of six pairs of refrigerants in the HTCHP system were compared theoretically at 100–170 °C discharge temperature and 55 °C evaporation temperature [3]. Implementing the HTCHP system, Ma [11] and Li [3] et al. adopted BY3A/BY3B and R245fa/BY6 as working fluid of LTS and HTS, respectively, the experimental results showed that the outlet water temperature of the HTCHP system could reach 142 °C and 168 °C. Among them, two scroll compressors were adopted for two stages by Ma et al. [11], and a scroll compressor and a piston compressor were adopted for the LTS and HTS by Li et al. [3]. Wang et al. [12] proposed extremum seeking control (ESC) as a model-free, real-time, optimizing control strategy for efficient operation of a cascade air source heat pump (CASHP). The CASHP system could provide condensing water of 85 °C with R404A and R245fa as the refrigerants for the LTS and HTS respectively.

In the past decades, the energy, exergy and economic analysis as well as the multi-objective optimum of the HTHP system have been widely investigated. Suleman et al. [13] performed comprehensive energy and exergy analyses of an integrated solar and heat pump system for industrial waste heat. The results showed that the energy efficiency and exergy efficiency were 58% and 75%, respectively. Pitarch et al. [14] carried out an exergy analysis on various components of the heat pump at different temperature lift. Based on the analysis, subcooling and superheat were chosen as objective functions to optimize the cycle's parameters. Farshi et al. [15] adopted thermo-economic analysis to evaluate the ejector boosted hybrid heat pump system. The results indicated that the system had a higher working domain and higher temperature lift in comparison with three other heat pumps (absorption, compression, and absorption/compression heat pumps). The feasibility of the air source heat pump saving the electrical energy consumption of the data center was investigated by Dashtebayaz et al. [16]. The 3E (energy-economic-environmental) analysis method was used to investigate the performance of the system, and the results indicated that the economic and environmental benefits were remarkable [16]. Fortes et al. [17] applied the thermo-economic methodology to allocate costs and environmental impact in a heat pump utilized for food dehydration and water production. Li et al. [18] used 4E (energy-exergy-economic-environmental) analysis method to evaluate the performance of an integrated system of HTHP and a gas-separation unit. The results demonstrated that the integrated system operated with high performance and provided significant economic and environmental benefits. Wu et al. [19] analyzed a novel dual-function heat pump and power generation integration system with 3E (energy-exergy-economic) and multi-objective optimum methods. The total cost and payback period of the system were chosen as the objective functions to obtain the optimum value, both of them were minimize type.

These literatures demonstrate that energy, exergy and economic analysis of single-stage HTHP systems have been widely studied. There is, however, still a lack of knowledge of HTCHP considering energy, exergy, economic and environmental (4E) analysis with multi-objective optimization. Unlike previous optimization researches on the HTCHP that focus only on the energy analysis and exergy analysis, the economic analysis, environmental analysis, the mathematical model and the multi-objective optimization of the HTCHP system have not been sufficiently discussed in the open literatures yet. Appropriate optimization strategies are necessary to improve the performance of HTCHP in terms of economy and energy efficiency. This paper designed an industrial HTCHP system for recovering the waste heat of the chemical plant and replacing the steam, using BY3B/BY6 as working fluids. Further, a mathematical

model of the HTCHP system considering 4E was established to aid in engineering and manufacture design applications. Additionally, to address the conflict between economic and energy aspects, multi-objective optimization of the system was conducted to determine optimal operating conditions. The optimization process was conducted based on NSGA-II technology and the optimal results were identified by the technique for order preference by similarity to an ideal solution (TOPSIS) decision-making method. The main contributions of this study include:

(1) The energy, exergy, economy and environment performance of a high-temperature cascade heat pump system with high compression ratio under different operating conditions are analyzed.
(2) Based on the simulation results, multi-objective optimization of the system is conducted and some optimal operational conditions are recommended.

2. Description of the high-temperature cascade heat pump system

The schematic diagram of the HTCHP system is presented in Fig. 1. The HTCHP system consists of two single-stage heat pumps. There are typically three cycles in the single-stage heat pump, namely a refrigerant cycle, heat source cycle and heat sink cycle. The equipment in the refrigerant cycle mainly includes an evaporator, compressor, condenser and electronic expansion valve (EEV). The low-temperature and low-pressure vapor is compressed in the compressor; and becomes overheated vapor with high temperature and high pressure. The vapor then passes into the condenser and is cooled by the heat sink. It becomes a saturated liquid with high temperature and pressure after the condenser. The liquid is continuously throttled in the EEV, enabling gas-liquid coexistence with low temperature and pressure. It then enters the evaporator to absorb the heat provided by the heat source, becoming a low temperature and low-pressure vapor, completing the refrigerant cycle of the single-stage heat pump. In the HTCHP system, two single-stage heat pumps are considered as LTS and HTS refrigerant cycles, respectively. Two cycles are connected by a cascade heat exchanger used as both the LTS condenser and HTS evaporator. The phase-change heat transfer occurs in both two-stage refrigerants in the cascade heat exchanger. In this paper, the waste heat with the temperature of 55–85 °C of the chemical enterprises was regarded as the heat source, the chemical materials of 140 °C that needed to be heated were treated as the heat sink, and the corresponding to the cascade temperature was 95–110 °C.

Two kinds of mixture refrigerants (BY3B/BY6) developed by our group [3] were selected as LTS and HTS refrigerants of the HTCHP system, respectively. The variations of enthalpy and entropy of BY3B and BY6 with temperature were shown in Fig. 2(a) and Fig. 2(b) of Ref. [3]. It should be noted that the ODPs are not zero (0.03 and 0.08) and the GWPs are 2125 and 670 [3]. Based on the Kyoto and Kigali Agreement as well as the F-gas regulation, such refrigerants are only temporarily used for analyzing the performance of the system at high temperature. Moreover, environmentally-friendly refrigerants with similar properties are being studied. Based on previous theoretical and experimental research, when the heating temperature was lower than 140 °C, the system had a good thermodynamic property.

In this system, open oil-free twin-screw compressors manufactured by Dandong Colossus were respectively selected in both stages of the cascade heat pump. The specific parameters are listed in Table 1 [20]. The compressors were selected under high temperature conditions for the following reasons: (1) The open type means that the motor and screw of the compressor are separated so the motor will not be destroyed due to high temperature of the refrigerant. (2) The male and female rotors of the oil-free twin-screw compressor mainly rely on synchronous gears to ensure the synchronous rotation, accurate alignment and no scraping at high discharge temperature. (3) In order to avoid damage to the compressor due to high temperature, the ratio of length and diameter of 1.35 was adopted, the tooth ratio of male and female rotors was 4:6, and the meshing clearance between rotors was widened to 0.25 mm to compensate for the rotors heat extension. In addition, oil-free are those in which the oil system and the compressed refrigerant are not in direct contact during the compression process. There is no lubricating oil between the compressor cavity and rotor, but the working parts (such as the gears, bearings) in the compressor are still lubricated. The compressor is sealed by oil seal and mechanical seal [21]. The schematic of the compressor is shown in Fig. 2. It should be noted that different types of compressors should be selected according to the specific working conditions.

2. Mathematical model

Fig. 3 shows the T-S diagram of the HTCHP system. The saturation lines of BY3B and BY6 are represented by purple and black curves in Fig. 3, respectively. The LTS and HTS cycle are shown by 0-1-2-3-4-5-6 (red line) and 0′-1′-2′-3′-4′-5′-6’ (green line), respectively. They all include four thermodynamic processes, namely

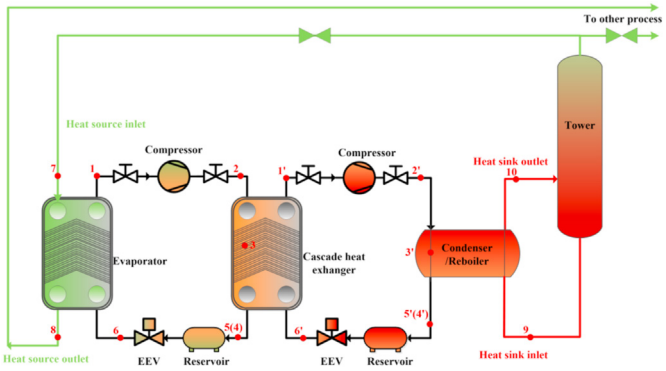

Fig. 1. Schematic diagram of the HTCHP system.

Fig. 2. Schematic of the open oil-free twin-screw compressor.

Table 1
The specific parameters of the compressor [20].

Equipment	Type	Manufacturer	Quantity	Specification
Open twin-screw compressor	KLY127.5−150	Dandong Colossus	2	The twin-screw compressor's suction volume is 8 m^3/min and its rotate speed is 3000 r/min, rated power is 150 kW. The maximum design temperature is 200 °C.
Variable Frequency Adjusting Speed 3-phase Induction Motor	YVFE2-280S-2	Hengshui electric Limited by Share Ltd	2	Rated power 150 kW, rotate speed is 3000 r/min, voltage is 380 V, triangle connection method.
Compressor lubrication oil pump	YE2-100L2-4	/	4	The rotate power is 3 kW, the frequency is 50Hz, and the rotate speed is 1440r/min.
Oil cooler	AL-8	/	2	The cooling area is 8 m^2, the design pressure is 3 MPa, and the design temperature is 110 °C.

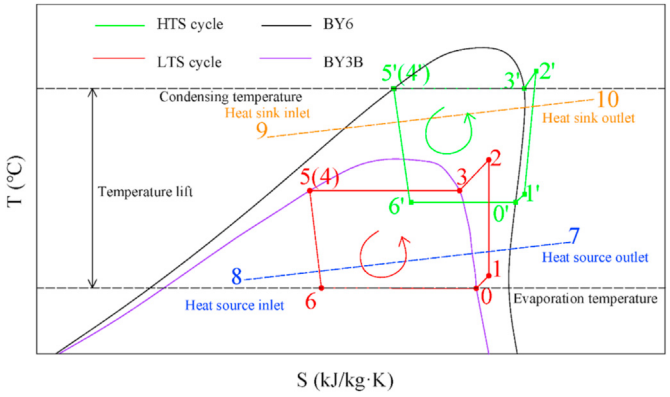

Fig. 3. T–S diagram of the HTCHP system.

evaporation, compression, condensation and throttling process. The blue line and orange line indicate the heat source and heat sink, respectively. The following physical assumptions were made:

(1) The heat loss of all components of the HTCHP system were considered negligible.
(2) The pressure drop of the heat exchanger and pipe were neglected.
(3) The throttle process in EEV was taken as isenthalpic, the isentropic of two compressors was assumed at 80% and the efficiency of the cascade heat exchanger was 80%.
(4) The outlet superheat degree of two evaporators was taken to be 3 °C and the outlet subcooling of two condensers, 0 °C. The average temperature difference between the HTS refrigerant and LTS refrigerant of the cascade heat exchanger was taken as 5 °C.
(5) The variation of kinetic energy, potential energy and chemical energy in thermal process were assumed to be zero.

2.1. Energy analysis

Based on the first law of thermodynamics, each component in the HTCHP system is regarded as a controlled unit, and the energy equation can be expressed as follows [22]:

$$\dot{Q} = \sum (\dot{m}h)_{out} - \sum (\dot{m}h)_{out} + \dot{W} \tag{1}$$

where, $\dot{Q}$ and $\dot{W}$ refer to the heat absorption and output technical work of the controlled unit in unit time, respectively; $\dot{m}$ and h represent the mass flow rate and the specific enthalpy of the fluid, respectively; the subscripts in and out respectively represent the inlet and outlet state of the controlled unit.

The specific energy balance equation of each component is shown in Table 2. η_s refers to the efficiency of the compressor. The subscripts L, H and f refer to the LTS, HTS and refrigerant, respectively.

The COP of the HTCHP system can be expressed by:

$$COP = \dot{Q}_{\mathrm{cond}} \Big/ \left(\dot{W}_{\mathrm{L}} + \dot{W}_{\mathrm{H}}\right) \tag{2}$$

2.2. Exergy analysis

Exergy destruction and exergy efficiency analysis were conducted as they were helpful to improve the performance of the HTCHP system. The reference state is defined at an ambient temperature of 20 °C and one atmospheric pressure. The exergy destruction is the difference between the inlet exergy and the outlet exergy and can be expressed as:

$$\dot{L}_{\mathrm{k}} = \dot{E}x_{\mathrm{in}} - \dot{E}x_{\mathrm{out}} \tag{3}$$

where, $\dot{L}$ refers to the exergy destruction in unit time. k refers to the component of the HTCHP system. $\dot{E}x$ is the enthalpy exergy of the fluid.

Table 2
Energy balance equations of each component.

Components	Energy balance equation
Evaporator	$\dot{Q}_{\mathrm{evap}} = \dot{m}_{\mathrm{L,f}}(h_1 - h_6) = \dot{m}_{\mathrm{waste-heat}}(h_7 - h_8)$
LTS compressor	$\dot{W}_L = \dot{m}_{L,f}(h_2 - h_1)/\eta_s$
Cascade heat exchanger	$\dot{Q}_{\mathrm{cas}} = \dot{m}_{\mathrm{L,f}}(h_2 - h_5)\eta_{\mathrm{cas}} = \dot{m}_{\mathrm{H,f}}(h_{1'} - h_{6'})$
LTS EEV	$h_5 = h_6$
HTS compressor	$\dot{W}_H = \dot{m}_{H,f}(h_{2'} - h_{1'})/\eta_s$
Condenser	$\dot{Q}_{cond} = \dot{m}_{H,f}(h_{2'} - h_{5'}) = \dot{m}_{chemical-material}(h_{10} - h_9)$
HTS EEV	$h_{5'} = h_{6'}$

Note: The numbers of these equations correspond to the Fig. 3, the same as follows.

Table 3
The exergy destruction and exergy efficiency equations of each component.

Components	Exergy destruction	Exergy efficiency
Evaporator	$\dot{Z}$	$\dot{Z} = \dot{Z}_{CI} + \dot{Z}_{OM}$
LTS compressor	$\dot{L}_{L,comp} = \dot{W}_L + \dot{m}_{L,f}[(h_1 - h_2) - T_0(s_1 - s_2)]$	$\psi_{L,comp} = \frac{\dot{m}_{L,f}[(h_2 - h_1) - T_0(s_2 - s_1)]}{\dot{W}_L}$
Cascade heat exchanger	$\dot{L}_{cas} = \dot{m}_{L,f}[(h_2 - h_5) - T_0(s_2 - s_5)] + \dot{m}_{H,f}[(h_{6'} - h_{1'}) - T_0(s_{6'} - s_{1'})]$	$\psi_{cas} = \frac{\dot{m}_{H,f}[(h_{1'} - h_{6'}) - T_0(s_{1'} - s_{6'})]}{\dot{m}_{L,f}[(h_2 - h_5) - T_0(s_2 - s_5)]}$
LTS EEV	$\dot{Z}_{OM}$	$\dot{Z}_k^{OM} = \phi \cdot \dot{Z}_k^{CI}$
HTS compressor	$\dot{L}_{H,comp} = \dot{W}_H + \dot{m}_{H,f}[(h_{1'} - h_{2'}) - T_0(s_{1'} - s_{2'})]$	$\psi_{H,comp} = \frac{\dot{m}_{H,f}[(h_{2'} - h_{1'}) - T_0(s_{2'} - s_{1'})]}{\dot{W}_H}$
Condenser	$Z_{evap} = 16000\left(\frac{A_{evap}}{100}\right)^{0.6}$	$Z_{L,comp} = 7364 \cdot m_{L,f} \cdot \left(\frac{P_2}{P_1}\right) \cdot \left(\frac{1-\eta_{comp}}{\eta_{comp}}\right)^{0.7}$
HTS EEV	$Z_{cas} = 16000\left(\frac{A_{cas}}{100}\right)^{0.6}$	$Z_{H,comp} = 7364 \cdot m_{H,f} \cdot \left(\frac{P_{2'}}{P_{1'}}\right) \cdot \left(\frac{1-\eta_{comp}}{\eta_{comp}}\right)^{0.7}$

The exergy efficiency of each component is the ratio of revenue exergy and payment exergy. It can be calculated by the following equation:

$$\psi_k = \frac{Ex_{revenue}}{Ex_{payment}} \tag{4}$$

where, the revenue exergy can be expressed by:

$$\dot{E}x_{revenue} = \dot{E}x_{payment} - \sum \dot{L}_k \tag{5}$$

therefore, the exergy efficiency can also be expressed as:

$$\psi_k = 1 - \frac{\sum \dot{L}_k}{\dot{E}x_{payment}} \tag{6}$$

The exergy destruction and exergy efficiency equations of each component of the HTCHP system are shown in Table 3.

The total exergy destruction and the exergy efficiency of the HTCHP system can be expressed as follows, respectively:

$$\dot{L} = \dot{L}_{evap} + \dot{L}_{L,comp} + \dot{L}_{cas} + \dot{L}_{L,EEV} + \dot{L}_{H,comp} + \dot{L}_{re} + \dot{L}_{H,EEV} \tag{7}$$

$$\psi = \frac{\dot{E}x_{revenue}}{\dot{E}x_{payment}} = \frac{\dot{Q}_{re}\left[1 - \frac{T_0}{(T_{10}-T_9)/\ln(T_{10}/T_9)}\right]}{\dot{Q}_{evap}\left[1 - \frac{T_0}{(T_7-T_8)/\ln(T_7/T_8)}\right] + \dot{W}_L + \dot{W}_H} = 1 - \frac{\dot{L}}{\dot{Q}_{evap}\left[1 - \frac{T_0}{(T_7-T_8)/\ln(T_7/T_8)}\right] + \dot{W}_L + \dot{W}_H} \tag{8}$$

2.3. Economic analysis

In the industrial field, new system applications are constrained not only by technical feasibility but also by economic performance [23]. This paper provided an analysis and decision-making method for enterprises to choose a new system by integrating thermodynamic processes and economic factors, taking into account the investment of equipment, operation and maintenance costs, and considering the exergy cost. For the steady-state and steady flow system in unit time, the annual cost rate and the unit exergy cost rate of the system can be established as follows:

$$\dot{C}_{product} = \dot{C}_{energy} + \dot{Z} \tag{9}$$

$$c_{product} = \frac{\dot{C}_{product}}{\dot{E}x_{revenue}} \tag{10}$$

where the energy cost rate is equal to the product of unit inlet energy exergy cost and payment exergy. That is $\dot{C}_{energy} = c_{energy}\dot{E}x_{payment}$. The non-energy cost rate $\dot{Z}$ includes the initial investment cost rate and operation and the project cost as well as maintenance cost rate. That is $\dot{Z} = \dot{Z}_{CI} + \dot{Z}_{PC} + \dot{Z}_{OM}$.

The initial investment cost rate $\dot{Z}_{CI}$ is given by:

$$\dot{Z}_k^{CI} = CRF \cdot Z_k^{CI} \tag{11}$$

where k refers to the component of the HTCHP system. Z_k^{CI} is the total initial investment of each component. *CRF* (Capital recovery factor) can be calculated as follows:

$$CRF = \frac{i(1+i)^n}{(1+i)^n - 1} \tag{12}$$

where the annual interest rate (i) is 15%, and the life time (n) of the system is 10 years [24].

In this paper, the reboiler of the revamped network of the chemical plant was directly treated as the condenser of the heat pump system, therefore, the cost of the condenser was not considered here.

The total cost of the equipment can be expressed:

$$\dot{Z}_{CI} = \sum \dot{Z}_k^{CI} \tag{13}$$

The calculation formula of initial investment cost of each component is given in Table 4. For the heat exchanger, the heat exchanger area (A) can be calculated by the formula $A = \frac{Q}{KF\Delta T_{LMTD}}$, here, Q refers to the heat exchange, K and F refer to the overall heat transfer coefficient (1200 W/(m^2·K) [25]) and to the correction factor of the logarithmic mean temperature difference (0.93 [26]) of the heat exchanger, respectively.

The project cost should be added to the non-energy cost rate of HTCHP system, which includes the unit installation (such as the piping, tank, instrumentation, and connection to the existing infrastructure) and other costs (such as the labor cost for the design, engineering and production processes, profits, and overheads). A multiplication factor is adopted to account for all these costs, that is [28]:

$$\dot{Z}_{PC} = 4.16 \cdot \dot{Z}_{CI} \tag{14}$$

In addition, the operation and maintenance cost rate $\dot{Z}_{OM}$ are

Table 4
The initial investment cost of each component.

Components	Equations	Ref
Evaporator	$Z_{evap} = 16000\left(\frac{A_{evap}}{100}\right)^{0.6}$	[15]
LTS compressor	$Z_{L,comp} = 7364 \cdot m_{L,f} \cdot \left(\frac{P_2}{P_1}\right) \cdot \left(\frac{1-\eta_{comp}}{\eta_{comp}}\right)^{0.7}$	[27]
Cascade heat exchanger	$Z_{cas} = 16000\left(\frac{A_{cas}}{100}\right)^{0.6}$	[15]
HTS compressor	$Z_{H,comp} = 7364 \cdot m_{H,f} \cdot \left(\frac{P_{2'}}{P_{1'}}\right) \cdot \left(\frac{1-\eta_{comp}}{\eta_{comp}}\right)^{0.7}$	[27]

given by:

$$\dot{Z}_k^{OM} = \phi \cdot \dot{Z}_k^{CI} \tag{15}$$

where ϕ is 0.06, which refers to the operation and maintenance factor [29].

This work took the annual net profit (ANP) and payback period (PP) as objective functions to analyze the economic performance of the HTCHP system. Without considering the profit of the waste heat and with considering the economic benefits of replacing high-temperature steam by the HTCHP system, the ANP and the PP can be expressed as:

$$ANP = \dot{m}_{steam} \cdot N \cdot \dot{Z}_{steam} - \dot{P} \cdot N \cdot \dot{Z}_{electricity} \tag{16}$$

$$PP = \frac{Z_{total}}{ANP} \tag{17}$$

where N represents the annual operation time of the system, generally taken as 8000 h/year. The mass flow rate of the steam is the ratio of the heating capacity and potential heat, which is $\dot{m}_{steam} = \dot{Q}_{re}/r_{steam}$.$\dot{P}$is the input power of the system. $\dot{Z}$represents the unit price corresponding to steam and electricity. The electricity and steam prices are shown in Table 5.

2.4. Environmental analysis

With growing concerns about environmental pollution and global warming, the rate of penalty cost of CO_2 emission should be considered. This is defined by Ref. [30]:

$$\dot{C}_{env} = \frac{\mu_{co_2} \times EC \times \frac{c_{co_2}}{1000}}{3600} \tag{18}$$

where μ_{co_2} and c_{co_2} are CO_2 avoid cost (0.88 kg/kW·h) and factor of emission (87 $/ton), respectively. *EC* is system annual electrical energy consumption.

2.5. Multi-objective optimization

The multi-objective optimization method has been employed in this paper, given that it can be used to optimize the HTCHP system based on two simultaneous objectives [31]. There is a Pareto frontier during the optimization procedure in which any objective function value will not be improved without lowering other target values [32]. The multi-objective optimization process comprises three parts: objective functions, constraints and decision variables [19]. The two conflicting objective functions in this paper are heating capacity (objective function-I) and ANP (objective function-II) which can be expressed as:

Objective function I: Heating capacity, Q_{cond} (maximize).

Objective function II: Annual net profit, ANP (maximize).

Heating capacity should be analyzed to evaluate the thermal performance of the HTCHP system, determined from Table 2 and explained in Section 3.1 under different operating conditions.

The ANP of the HTCHP system under different working conditions was determined from Eq. (16) as explained in Section 3.3.

There are three cases of the optimization process, namely heating capacity single-objective optimization, ANP single-objective optimization and multi-objective optimization. Variables were chosen based on minimizing or maximizing objective functions, maximized when the variables were at the optimal values [19]. The constraints consisted of equality and inequality constraints. Equality constraints were formulated with an energy model, and inequality constraints permitted the operational conditions inside safe limitations. The proposed HTCHP system had one decision variable (heat source inlet temperature) and the constraints were optimized by the NSGA-II technology, which is an effective method to search for optimal solutions of multi-objective optimization, introduced by Deb in 2002 [33]. The details of the NSGA-II technology and its pseudo-codes were reported by Jain [34]. Non-dominated results include Pareto frontier, in which any value of the objective functions cannot be improved without lowering some other objective values [32]. Therefore, a decision-making method of TOPSIS was necessary to look for optimal solutions from the Pareto frontier. Sayyaadi et al. [35] recommended that both heating capacity and ANP were in normalized form. The following fuzzy method was applied to conduct the non-dimensionalization process of heating capacity and annual net profit, as defined by Eqs. (19) and (20).

$$Q_{cond.i}^{n} = \frac{Q_{cond.i} - \min(Q_{cond.i})}{\max(Q_{cond.i}) - \min(Q_{cond.i})} \tag{19}$$

$$ANP_i^n = \frac{ANP_i - \min(ANP_i)}{\max(ANP_i) - \min(ANP_i)} \tag{20}$$

To find optimal solutions, the TOPSIS decision-making method was applied during the optimization process. The TOPSIS method is a multi-objective decision making method. The principal of the method is to define the ideal point and the non-ideal point of the decision-making problem to find the optimal point in the feasible solution. The optimal point is closest to the ideal point and furthest from the negative ideal point [36]. The non-ideal point and ideal

Table 5
The electricity and steam price.

Project	Value	Unit
Electricity price of own power plant	0.05	$/kW·h
Electricity price of the Ref. [28]	0.086	$/kW·h
Steam price of own power plant	17.18	$/ton
External steam price	27.92	$/ton

point are hypothetical points with the minimum or maximum heating capacity and annual net profit. The distance of any points on the Pareto frontier from the ideal and non-ideal points can be measured by Eqs. (21) and (22) [37].

$$d_{i+} = \sqrt{\left(Q^{n}_{cond.i} - Q^{n,ideal}_{cond}\right)^2 + \left(ANP^{n}_{i} - ANP^{n,ideal}\right)^2} \tag{21}$$

$$d_{i-} = \sqrt{\left(Q^{n}_{cond.i} - Q^{n,non-ideal}_{cond}\right)^2 + \left(ANP^{n}_{i} - ANP^{n,non-ideal}\right)^2} \tag{22}$$

The proximity index is calculated as [38]:

$$Cl_i = \frac{d_{i-}}{d_{i+} + d_{i-}} \tag{23}$$

If both heating capacity and ANP are ideal points of the Pareto frontier, Cl_i will be 1. If they are non-ideal points, Cl_i will be 0. The point with maximum Cl_i will be chosen as the final result. The optimization flowchart is shown in Fig. 4.

2.6. System specification

In this section, a case study was conducted to analyze the thermodynamic and the economic performances of the HTCHP system, using the mathematical model proposed above. The thermodynamic design conditions and economic parameters of HTCHP are shown in Table 6 and the tuning parameters of the NSGA-II method used in the optimization process are shown in Table 7. Similar tuning parameters have been used in the multi-objective optimization of vapor absorption heat pumps [34]. The details of NSGA-II technology along with the code is listed in their Appendix.

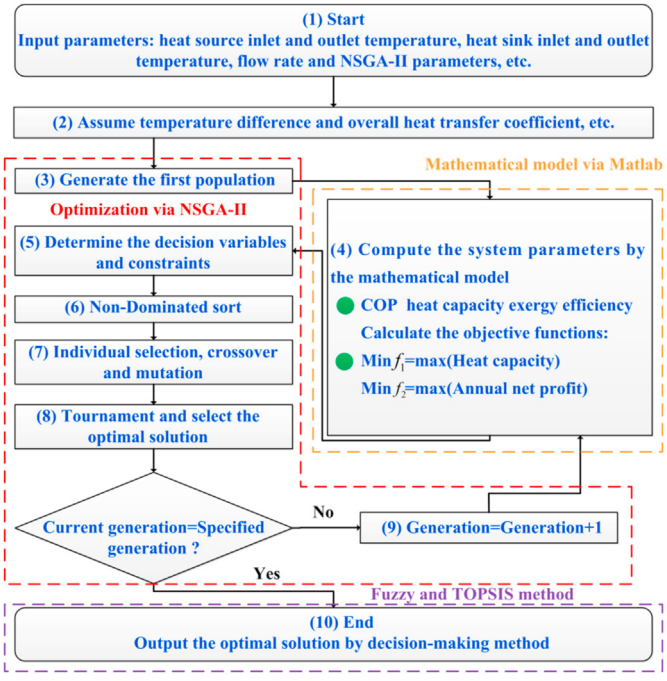

Fig. 4. Flowchart of Multi-objective optimal for the optimal solution.

Table 6
Thermodynamic design conditions and economic parameters used in mathematical model.

Parameters	Value
Heat source inlet temperature T_7 (°C)	70
Heat source outlet temperature T_8 (°C)	63
Evaporating temperature T_{evap} (°C)	60
Condensing temperature T_{cond} (°C)	145
Cold source inlet temperature T_9 (°C)	135
Cold source outlet temperature T_{10} (°C)	140
Heat absorption Q_{evap}(kW)	418
Overall heat transfer coefficient of the heat exchangers K [W/(m^2·K)]	1200
Emission factor of electricity in China μ_{co_2} (kg/kW·h)	0.88
Cost of CO_2 avoided c_{co_2} ($/ton)	87
Degree of superheating of refrigerant at evaporator outlet (°C)	3
Degree of subcooling of refrigerant at condenser outlet (°C)	0

Table 7
Parameters considered in optimization process [34].

Tuning parameters	Value
Population size	200
Maximum number of generations	500
Probability of crossover	0.85
Probability of mutation	0.1
Selection process	Tournament
Tournament size	2

3. Results and discussion

3.1. Results of energy analysis

The variations of two stages input power, heating capacity and COP with heat source inlet temperature are shown in Fig. 5 when the heat absorption was fixed 418 kW and the condensing temperature at 145 °C. Fig. 5(a) shows that input power at LTS and HTS of the HTCHP system decreased with the increase of the heat source inlet temperature. When the temperature increased by 1 °C, the input power of the LTS and HTS decreased by 1.3% and 1.8%, respectively. The decreasing trend of input power in HTS was higher than that of the LTS, which was due to the combined effect of the mass flow rate of the working fluid and the specific enthalpy difference at the inlet and outlet of the compressors. Under the same working condition, the mass flow rate and specific enthalpy difference of the HTS were smaller than those of the LTS. The mass flow rate of the LTS showed an upward trend, while that of HTS was the opposite. The specific enthalpy difference trended downward.

Fig. 5(b) shows the variations of heating capacity and COP of the HTCHP system with the heat source temperature. It should be noted that the heating capacity of the cascade heat exchanger is the average value of LTS heating capacity and HTS heat absorption. As the heat source temperature increased from 55 °C to 85 °C, the heating capacity of the system and the cascade heat exchanger decreased gradually, and the variation trend of the former was more violent than that of the latter, while COP increased gradually. When the heating absorption of the system was constant, the heating capacity decreased with the decrease of the inlet power. The COP rise can be explained from two perspectives: (1) mathematically, the reduction rate (14.2%) of the heating capacity was lower than the growth rate (36.9%) of total inlet power; (2) thermodynamically, this was consistent with the theory of inverse Carnot cycle. The heat sink temperature was constant, with the increase of the heat source inlet temperature, the temperature lift (the temperature difference of heat source and heat sink) was reduced, corresponding to the COP increase. The COP of the HTCHP

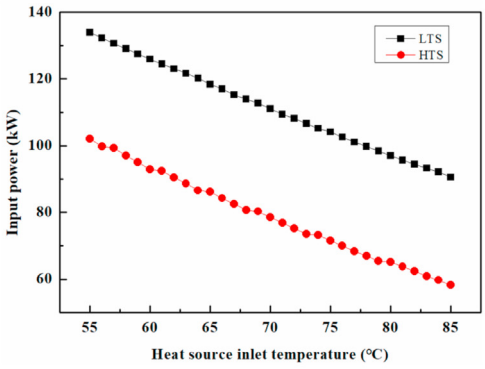

(a) Input power-Heat source inlet temperature

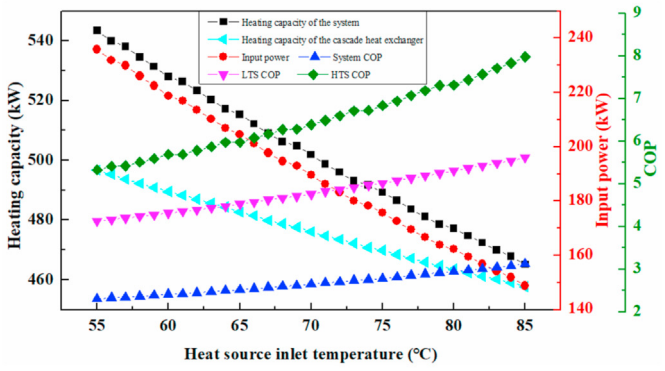

(b) Heating capacity and COP-Heat source inlet temperature

Fig. 5. Variations of input power, heating capacity and COP with heat source inlet temperature.

system reached a maximum of 3.1 at 85 °C and reached a minimum of 2.3 at 55 °C. In the two refrigerant cycles, the heating capacity of the HTS was higher than that of the LTS, and the inlet power was opposite. This double effect resulted in the COP of the HTS being higher than that of the LTS.

3.2. Results of exergy analysis

On the basis of the exergy analysis, the results of the exergy destruction and exergy efficiency are shown in Fig. 6. Fig. 6(a) shows that the exergy destruction of the cascade heat exchanger increased with the increase of the heat source inlet temperature, which was different from other components. This can be explained by the rate of exergy destruction increase of the LTS condenser being higher than the rate of destruction decrease of the HTS evaporator. In the LTS cycle, the exergy destruction of EEV was the largest, followed by compressor. The heat source inlet temperature had a negative correlation with the exergy destruction of the EEV and compressor, the destruction decreased with the increase of temperature. When the temperature increased by 1 °C, the exergy destruction of the LTS compressor decreased by 2.0%, which was higher than the 1.0% of the LTS EEV. The exergy destruction of the evaporator was the smallest, and was basically unchanged at 3.8 ± 0.4 kW. In the HTS cycle, the exergy destruction of the EEV and compressor was also the largest. The trend with the heat source inlet temperature was similar to that of the LTS. When the temperature increased by 1 °C, the exergy destruction of the HTS compressor decreased by 1.8%, which was lower than the 2.6% of the HTS EEV. The exergy destruction of the condenser was the smallest, and basically unchanged at 6.3 ± 0.5 kW. This was due to

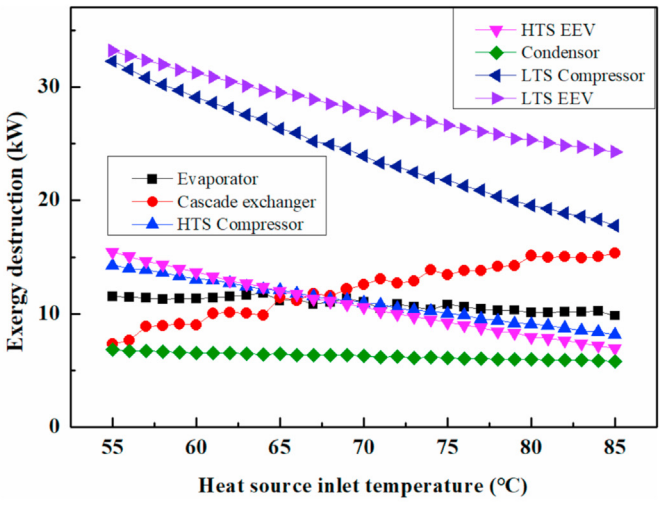

(a) Exergy destruction-Heat source inlet temperature

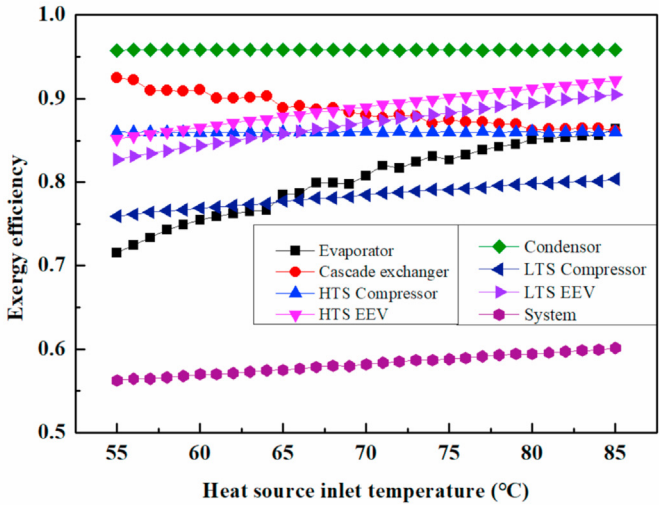

(b) Exergy efficiency-Heat source inlet temperature

Fig. 6. Variations of exergy destruction and exergy efficiency with heat source inlet temperature.

the exergy destruction of cooling capacity of the condenser being large, and the difference of enthalpy exergy being small.

Fig. 6(b) shows that the total exergy efficiency of the HTCHP system increased from 56.3% up to 60.1% with the increase of the heat source inlet temperature. Furthermore, the exergy efficiency of each component of the HTCHP system changed with the heat source inlet temperature in the opposite direction to the exergy destruction. In the HTCHP system, the exergy efficiency of the LTS compressor was the smallest, which increased from 77.4% to 80.4% as the heat source inlet temperature is more than 64 °C. The exergy efficiency of the HTS EEV was the smallest, and increased from 85.2% to 92.2% as the heat source inlet temperature increased. The LTS compressor and HTS EEV should be considered a priority in the optimization of the HTCHP system. The exergy efficiency of condenser remained at 92%. The exergy efficiency of the condenser was the largest and the exergy destruction was the smallest, which was conducive to the reconstruction of the reboiler in industrial applications.

The exergy destruction of the LTS was higher than that of the

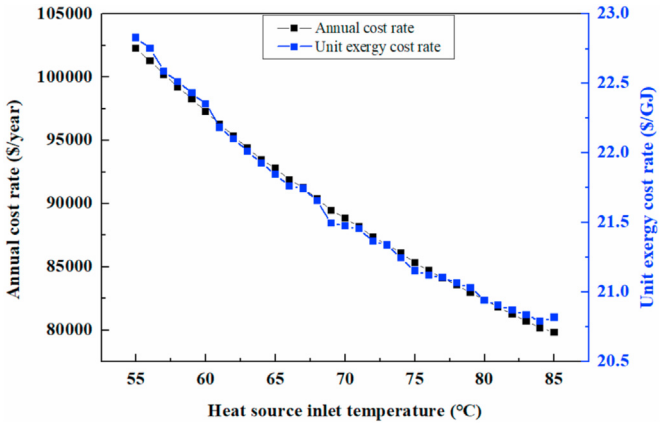

Fig. 7. Variations of annual cost rate and unit exergy cost rate with heat source inlet temperature.

HTS, and the exergy efficiency was opposite without considering the cascade heat exchanger. This was due to the superior performance of BY6 in comparison to BY3B. Therefore, the development of LTS working fluid with excellent performance may prove to be a promising research direction.

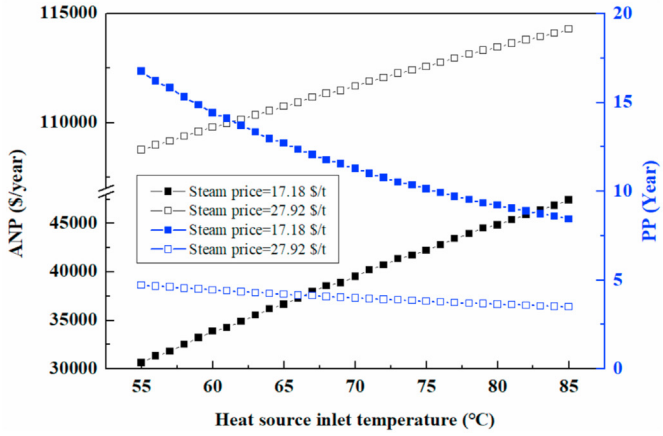

(a) ANP and PP -Heat source inlet temperature (Electricity price=0.05 $/kW·h)

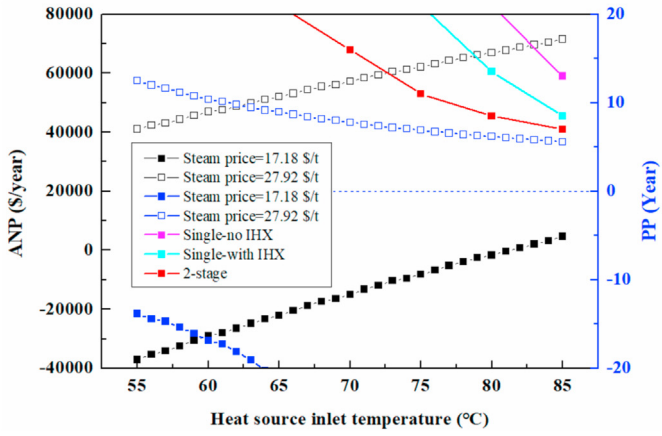

(b) ANP and PP-Heat source inlet temperature (Electricity price=0.086 $/kW·h).

Fig. 8. Variations of annual net profit and payback period with heat source inlet temperature, electricity and steam price.

3.3. Results of economic analysis

The trend of annual cost rate and unit exergy cost rate of the system with heat source inlet temperature is shown in Fig. 7. Both the annual cost rate and the unit exergy cost rate gradually decreased with the increase of the inlet temperature. The performance of the system improved synchronously with an increase in the heat source inlet temperature, followed by a decrease in initial investment cost rate, and finally a reduction in the annual cost rate. The maximum deviation between the maximum and minimum value of the unit exergy cost rate was less than 5.8%. This means that the heat source inlet temperature had little effect on the unit exergy cost rate.

Fig. 8 (a) and (b) show the variation of ANP and PP of the system with the heat source inlet temperature for different steam prices (17.18 $/t and 27.92 $/t) and electricity prices (0.05 $/kW·h and 0.086 $/kW·h), respectively. As shown in Fig. 8(a), when the electricity price was equal to 0.05 $/kW·h, the ANP increased with the heat source inlet temperature. The higher the steam price, the more obvious the ANP and the shorter the PP. The maximum ANP reached 114294.9 $/year, the minimum PP was 3.5 years at a heat source inlet temperature of 85 °C and the steam price was 27.92 $/t. At the steam price of 27.92 $/t and the electricity price of 0.05 $/kW·h, the PP of the whole system is less than 5 years, which is reasonable for enterprises. At the steam price of 17.18 $/t, Fig. 8(b) shows different trends compared with Fig. 8(a), ANP becomes positive only when the heat source inlet temperature is more than 82 °C, and the PPs are not shown in the Fig. 8(b) due to they exceed the maximum ordinate value. It shows that it is not suitable to apply HTCHP system to transform the original system in this condition. In addition, the performance of HTCHP system with BY3B/BY6 in this paper and that of the single-stage heat pump (without and with the inter heat exchanger (IHE)) as well as 2-stage heat pump system with R1234ze (z) as the circulating working fluid proposed by Kosmadakis et al. [28] are compared in Fig. 8(b). The results show that the PPs of four different systems are 5.6, 13, 8.5 and 7 years respectively under the condition of 85 °C heat source inlet temperature and the same electricity price. Although the steam price in this paper is not consistent with gas price proposed by Kosmadakis et al. [28], it can be considered that the calculation in this paper is reasonable. In summary, an interesting phenomenon can be summarized as follows: the higher the steam price, the lower the electricity price, the more favorable for the transformation of the original system. This will need to be confirmed with concrete economic performance analysis.

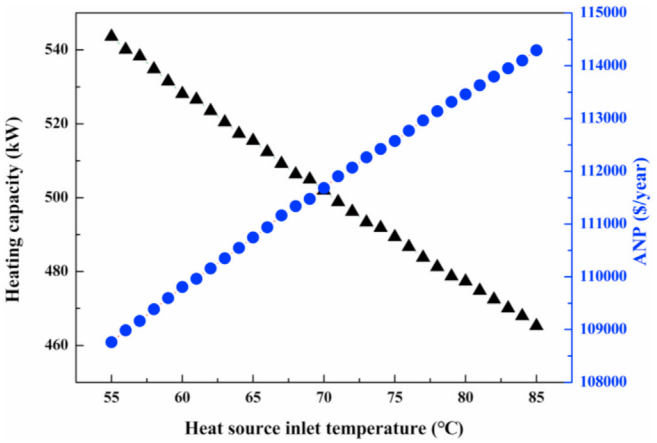

Fig. 9. Heating capacity and ANP of the system.

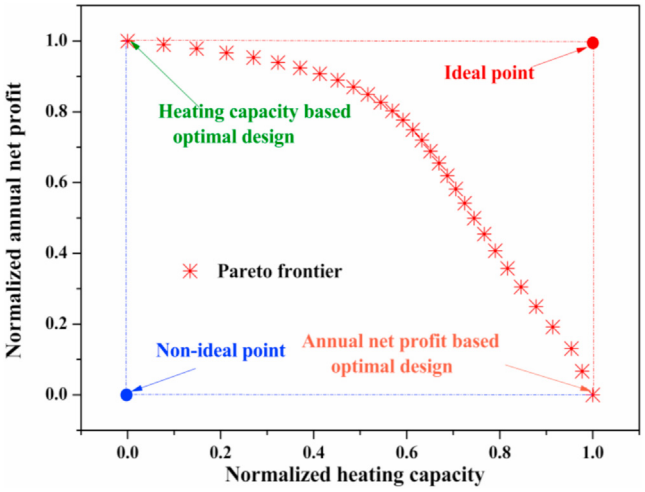

Fig. 10. Pareto frontier with normalized form in multi-objective process.

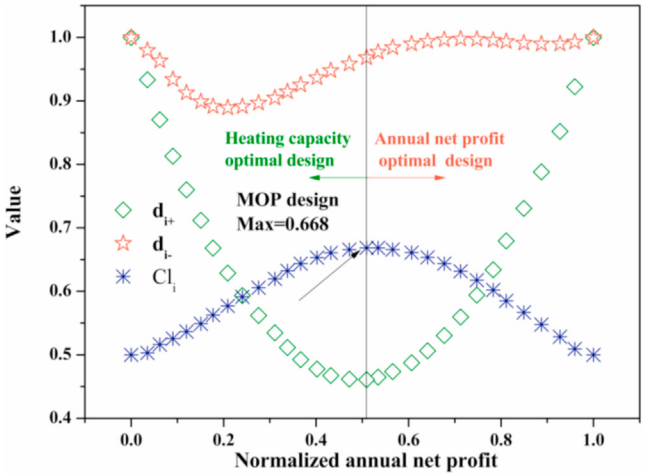

Fig. 11. The values in TOPSIS method.

3.4. Results of multi-objective optimization

Fig. 9 shows both heating capacity and ANP of the HTCHP at different heat source inlet temperature. As shown in Fig. 9, the ANP increased and the heating capacity decreased with increasing heat source inlet temperature. As previously mentioned, a system with high heating capacity may have low ANP, and a system with high ANP may have low heating capacity, so both are not optimal. Here, this issue can be solved by using the multi-objective optimization method. The Pareto frontier with normalized form using the NSGA-II technology in multi-objective optimization is shown in Fig. 10, where the heat source inlet temperature increased from 55 to 85 °C and the condensing temperature was 145 °C. Normalized heating capacity and normalized ANP were calculated according to Eqs. (19) and (20). When the heat source inlet temperature increased from 55 to 85 °C, the maximum and minimum heating capacity and ANP could be obtained from Fig. 9 to calculate the normalized heating capacity and normalized ANP at every point. From Fig. 10, the ideal point was found at the normalized ANP and the normalized heating capacity values of 1. According to Eqs. (19) and (20), both heating capacity and ANP were at a maximum under this condition. However, it should be noted that the existence of this ideal point is not practically possible. The non-ideal point is found when the normalized heating capacity and the normalized ANP are 0. When the normalized ANP is 1 and the normalized heating capacity is 0, the system is an ANP-based optimal design. When the normalized heating capacity is 0 and the normalized ANP is 1, the system is a heating capacity-based optimal design. To search for the optimal results in the Pareto frontier, the TOPSIS decision-making method was also applied.

According to the Eqs. 21–23, the d_{i+}, d_{i-} and Cl_i of every point were calculated and a point with the maximum proximity index Cl_i was chosen as the optimal result. Fig. 11 shows the variation of d_{i+}, d_{i-} and Cl_i with normalized ANP when the heat source inlet temperature increased from 55 to 85 °C and the condensing temperature was 145 °C. It is shown that both d_{i+} and d_{i-} decreased first before increasing under different heat source inlet temperature. The Cl_i can be calculated by d_{i+} and d_{i-} which increased at the beginning and then started to decrease. From Fig. 11, the maximum Cl_i was 0.668 at the normalized ANP of 0.32 at the heat source inlet temperature of 71 °C. In this optimal solution, the ANP was 111905.6 $/year and the heating capacity was 498.9 kW. From Fig. 11, any points of the Pareto frontier located on the left-hand side of the maximum Cl_i indicate better thermal performance. Those points located on the right-hand side, however, indicate better economic performance.

Table 8 shows ANP, normalized ANP, heating capacity and normalized heating capacity in both single-objective optimization and multi-objective optimization processes. It should be noted that

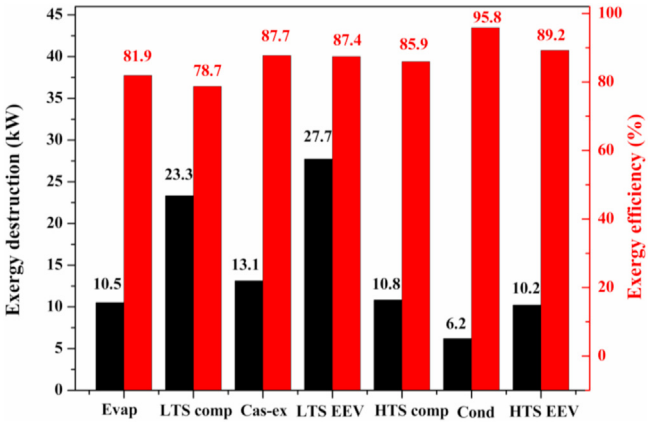

Fig. 12. Exergy analysis of the system under optimal condition at the heat source inlet temperature of 71 °C.

Table 8
Heating capacity and ANP value under three optimization procedures.

Optimization parameters	Q_{cond} (kW)	ANP ($/year)	$Q^n_{cond.i}$	ANP^n_i
Design condition	501.9	111684.6	0.688	0.651
Single-objective optimization of heating capacity	543.6	108762.3	1	0
Multi-objective optimization	498.9	111905.6	0.719	0.633
Single-objective optimization of annual net profit	465.3	114294.8	0	1

Table 9
Thermodynamic conditions in different processes.

Parameters	Design condition	Single-objective optimization of heating capacity	Multi-objective optimization	Single-objective optimization of ANP
$\dot{P}_L$ (kW)	111.1	133.9	109.4	90.6
$\dot{P}_H$ (kW)	78.6	102.1	76.9	58.3
COP (LTS)	4.7	4.1	4.8	5.6
COP (HTS)	6.4	5.3	6.4	7.9
COP (overall)	2.7	2.3	2.6	3.1
Compress ratio (LTS)	2.4	3.1	2.4	2.0
Compress ratio (HTS)	2.3	2.7	2.2	1.9
PP (year)	3.9	4.7	3.8	3.5

if any of the heating capacity based optimized design or ANP based optimized design was selected, the design would inadequately meet other conditions. According to Table 8, for the single-objective optimization of heating capacity as an optimal design, the average ANP was 4.8% lower than its maximum possible value; whereas, for the single-objective optimization of annual net profit, the average heating capacity was 14.4% lower than its maximum possible value. In addition, if the multi-objective optimization design was selected as the final solution, the average ANP and heating capacity were 2.8% and 6.7% lower than their maximum possible values. Therefore, multi-objective optimization design was proved more favorable than other single-objective optimization designs. Fig. 12 shows the results from the exergy analysis of the optimal condition and some thermodynamic parameters concerned with system performance are listed in Table 9. As reflected in Fig. 12, LTS EEV was the biggest contributor to the exergy destruction, caused by the large temperature difference.

The main aim of this paper was to investigate the thermal and economic performance, ANP and heating capacity of the HTCHP system, and to find the optimal solution by a multi-objective optimization method improving these performances of the system. However, three limitations in this paper should be noted. First, the results discussed above were based on theoretical analysis which should be verified by experiments. Second, the scale of the system is small and no mature industrial application presently exists. Last, the thermal performance of the system with working fluids in this paper may not be optimal. Therefore, the system with a heating capacity over 1 MW should be examined experimentally and additional appropriate working fluids for better system performance should be investigated.

4. Conclusion

In this study, a high-temperature cascade heat pump system for recovering the waste heat of the chemical plant and replacing the steam has been designed. A mathematical model, considering energy, exergy, economy and environment, has been developed under different heat source inlet temperature to analyze the thermodynamic and the economic performance of the HTCHP. Both multi-objective optimization and the TOPSIS decision-making method were applied to search for the optimal design and operation states of the HTCHP system, with maximized heating capacity and ANP. The main conclusions from this paper can be summarized as followings:

(1) For the HTCHP system, its COP and exergy efficiency increased with increasing heat source inlet temperature, but not with increasing heating capacity. When heat source inlet temperature was 85 °C, the maximized COP and exergy efficiency of the whole system were 3.1 and 60.1%, respectively.
(2) A higher heating capacity of the system may lead to lower ANP, and vice versa. Neither were optimal designs. When the heat source inlet temperature was 85 °C, the maximum ANP was 114294.9 $/year under the condition of 0.05 $/kW·h electricity price and 27.92 $/t steam price, the minimum heating capacity was 465.3 kW; when the heat source inlet temperature was 55 °C, the minimum ANP was 108762.3 $/year and the maximum heating capacity was 543.6 kW in the same situation.
(3) At the steam price of 27.92 $/t and the electricity price of 0.05 $/kW·h, the PP of the whole system is less than 5 years, which is reasonable for enterprises. Usually, the higher the steam price, the lower the electricity price, the more favorable for the transformation of the original system. However, this still needs to be confirmed with concrete economic performance analysis in practice.
(4) The system was optimized by solving the conflict between heating capacity and ANP, using the multi-objective optimization method. According to the optimization, when the multi-objective optimization design was chosen as the final result, the average heating capacity and the average ANP were 2.8% and 6.7% lower than their maximum possible values, respectively. These optimization results have better performance than the single-objective optimization.

Credit author statement

Zhangxiang Wu: Writing and software. Xiaoyan Wang: Data curation, Figure. Sha Li: Software and investigation. Xiaoqiong Li: Writing, method, reviewing and editing. Xiaochen Yang: method, reviewing and editing. Xuelian Ma: reviewing and editing. Yufeng Zhang: Supervision.

Declaration of competing interest

The authors declare that they have no known competing financial interests or personal relationships that could have appeared to influence the work reported in this paper.

Acknowledgement

The authors would like to express their thanks to the supporters of the 973 National Basic Research Program of China (No. 2015CB251403) and Postdoctoral funded project of advanced discipline construction of Engineering Science.

References

[1] Wu Z, Zhang Y, Deng N. Performance investigation of the heat pump and power generation integration system. INT J ENERG RES 2019;43(14).
[2] Imran M, Usman M, Park BS, Lee DH. Volumetric expanders for low grade heat and waste heat recovery applications. Renew Sustain Energy Rev 2016;57:1090–109.
[3] Li X, Zhang Y, Ma X, Deng N, Jin Z, Yu X, et al. Performance analysis of high-temperature water source cascade heat pump using BY3B/BY6 as

refrigerants. Appl Therm Eng 2019;159:113895.
[4] Arpagaus C, Bless F, Uhlmann M, Schiffmann J, Bertsch SS. High temperature heat pumps: market overview, state of the art, research status, refrigerants, and application potentials. ENERGY 2018;152:985–1010.
[5] Wu D, Jiang J, Hu B, Wang RZ. Experimental investigation on the performance of a very high temperature heat pump with water refrigerant. ENERGY 2019;190:116427.
[6] Jain PKBS. Cascade systems: past, present, and future. Build Eng 2007;113:245–52.
[7] Rezayan O, Behbahaninia A. Thermoeconomic optimization and exergy analysis of CO2/NH3 cascade refrigeration systems. ENERGY 2011;36:888–95.
[8] Song Y, Li D, Cao F, Wang X. Theoretical investigation on the combined and cascade CO2/R134a heat pump systems for space heating. Appl Therm Eng 2017;124:1457–70.
[9] Song Y, Ye Z, Wang Y, Cao F. The experimental verification on the optimal discharge pressure in a subcooler-based transcritical CO2 system for space heating. ENERG BUILDINGS 2018;158:1442–9.
[10] Bamigbetan O, Eikevik TM, Nekså P, Bantle M, Schlemminger C. Experimental investigation of a prototype R-600 compressor for high temperature heat pump. ENERGY 2019;169:730–8.
[11] Ma X, Zhang Y, Li X, Zou H, Deng N, Nie J, et al. Experimental study for a high efficiency cascade heat pump water heater system using a new near-zeotropic refrigerant mixture. Appl Therm Eng 2018;138:783–94.
[12] Wang W, Li Y, Hu B. Real-time efficiency optimization of a cascade heat pump system via multivariable extremum seeking. Appl Therm Eng 2020;176:115399.
[13] Suleman F, Dincer I, Agelin-Chaab M. Energy and exergy analyses of an integrated solar heat pump system. Appl Therm Eng 2014;73:559–66.
[14] Pitarch M, Hervas-Blasco E, Navarro-Peris E, Corberán JM. Exergy analysis on a heat pump working between a heat sink and a heat source of finite heat capacity rate. Int J Refrig 2019;99:337–50.
[15] Farshi LG, Khalili S. Thermoeconomic analysis of a new ejector boosted hybrid heat pump (EBHP) and comparison with three conventional types of heat pumps. ENERGY 2019;170:619–35.
[16] Deymi-Dashtebayaz M, Valipour-Namanlo S. Thermoeconomic and environmental feasibility of waste heat recovery of a data center using air source heat pump. J Clean Prod 2019;219:117–26.
[17] Fortes AFC, Carvalho M, Da Silva JAM. Environmental impact and cost allocations for a dual product heat pump. ENERG CONVERS MANAGE 2018;173:763–72.
[18] Li X, Zhang Y, Fang L, Jin Z, Zhang Y, Yu X, et al. Energy, exergy, economic, and environmental analysis of an integrated system of high-temperature heat pump and gas separation unit. ENERG CONVERS MANAGE 2019;198:111911.
[19] Wu Z, Zhang Y, Sheng Y. Energy, exergy, economic(3E) analysis and multi-objective optimization of a novel dual functional integration system. ENERG CONVERS MANAGE 2019;199:111962.
[20] Li X, Wang X, Zhang Y, Fang L, Deng N, Zhang Y, et al. Experimental and economic analysis with a novel ejector-based detection system for thermodynamic measurement of compressors. APPL ENERG 2020;261:114395.
[21] Shang Y. Main structure and design of oil-free screw compressor. Compressor technology. In Chinese 2008;2:28–30.
[22] Yao S, Zhang Y, Yu X. Thermo-economic analysis of a novel power generation system integrating a natural gas expansion plant with a geothermal ORC in Tianjin, China. ENERGY 2018;164:602–14.
[23] Du F. Thermoeconomics research of a large reclaimed water source heat pump central heating system. Hebei University of Engineering, In Chinese; 2013.
[24] Jain V, Sachdeva G, Kachhwaha SS. NLP model based thermoeconomic optimization of vapor compression–absorption cascaded refrigeration system. Energy Convers Manag 2015;93:49–62.
[25] Roetzel W, Spang B. C3 typical values of overall heat transfer coefficients. Berlin Heidelberg: Springer-Verlag; 2010. p. 75–8.
[26] El-Said EMS, Abou Al-Sood MM. Shell and tube heat exchanger with new segmental baffles configurations: a comparative experimental investigation. Appl Therm Eng 2019;150:803–10.
[27] Mehr AS, Zare V, Mahmoudi SMS. Standard GAX versus hybrid GAX absorption refrigeration cycle: from the view point of thermoeconomics. ENERG CONVERS MANAGE 2013;76:68–82.
[28] Kosmadakis G, Arpagaus C, Neofytou P, et al. Techno-economic analysis of high-temperature heat pumps with low-global warming potential refrigerants for upgrading waste heat up to 150 °C[J]. Energy Convers Manag 2020;226:113488. https://doi.org/10.1016/j.enconman.2020.113488.
[29] Liu S, Li Z, Dai B, Zhong Z, Li H, Song M, et al. Energetic, economic and environmental analysis of air source transcritical CO2 heat pump system for residential heating in China. Appl Therm Eng 2019;148:1425–39.
[30] Mosaffa AH, Farshi LG, Ferreira CAI, Rosen MA. Exergoeconomic and environmental analyses of CO2/NH3 cascade refrigeration systems equipped with different types of flash tank intercoolers. ENERG CONVERS MANAGE 2016;117:442–53.
[31] Wu Z, Sha L, Zhao M, Wang X, Ma H, Zhang Y. Performance analyses and optimization of a reverse Carnot cycle-organic Rankine cycle dual-function system. ENERG CONVERS MANAGE 2020:212.
[32] Wang YZ, Zhao J, Wang Y, An QS. Multi-objective optimization and grey relational analysis on configurations of organic Rankine cycle. Appl Therm Eng 2017;114:1355–63.
[33] Deb K, Agrawal S, Pratap A, Meyarivan T. A fast elitist non-dominated sorting genetic algorithm for multi-objective optimization: NSGA-II. Springer Berlin Heidelberg; 2000.
[34] Jain V, Sachdeva G. Energy, exergy, economic (3E) analyses and multi-objective optimization of vapor absorption heat transformer using NSGA-II technique. ENERG CONVERS MANAGE 2017;148:1096–113.
[35] Sayyaadi H, Nejatolahi M. Multi-objective optimization of a cooling tower assisted vapor compression refrigeration system. Int J Refrig 2011;34:243–56.
[36] Ahmadi MH, Sayyaadi H, Mohammadi AH, Barranco-Jimenez MA. Thermo-economic multi-objective optimization of solar dish-Stirling engine by implementing evolutionary algorithm. Energy Convers Manag 2013;73:370–80.
[37] Wu Z, Sha L, Yang X, Zhang Y. Performance evaluation and working fluid selection of combined heat pump and power generation system (HP-PGs) using multi-objective optimization. ENERG CONVERS MANAGE 2020:221.
[38] Wu Z, Wang Y, You S, Zhang H, Zheng X, Guo J, et al. Thermo-economic analysis of composite district heating substation with absorption heat pump. Appl Therm Eng 2020;166:114659.